# Directing the self-assembly of multiple DNA nanostructures in a single reaction

Thesis

Presented in Partial Fulfillment of the Requirements for the Degree Bachelors of Science in the

Undergraduate School of The Ohio State University

By

Vasiliki Kolliopoulos

Undergraduate Program in Chemical and Biomolecular Engineering
Research Distinction in Mechanical and Aerospace Engineering

The Ohio State University

2018

Thesis Committee

Dr. Carlos E. Castro, Advisor, Department of Mechanical and Aerospace Engineering

Dr. James Lee, Department of Chemical and Biomolecular Engineering

Abstract

DNA origami is a programmable self-assembly technique that combines a long single-stranded DNA template strand with hundreds of shorter custom DNA strands (called “staples”) to fabricate nanostructures in a bottom-up assembly process. These nanostructures are designed with unprecedented geometric precision and have demonstrated tremendous promise for applications in cancer therapeutics, biosensors, nanorobotics and more. However, the intricacies of the DNA origami folding process are not well-understood although they have been a subject of much research. Currently, higher order assemblies are formed in a multi-step polymerization processes. Forming multiple, different types of nanostructures in one step could allow for more efficient assembly of complex mechanisms; however, recent studies show this method tends to produce chimeras, which include features of different designs within a single structure. The purpose of this study is to characterize the parameters for fine-tuning the self-assembly folding process to simultaneously fold two or more unique structures while minimizing chimeras and aggregation. Using two structures, a 6-helix bundle and an 18-helix bundle, that exhibit similar annealing temperatures, we explored the effect of adjusting the staple concentration of each structure during folding. By adjusting the staple concentrations we can bias the folding toward either structure and adjust relative yields ranging from all 6-helix bundle, to varying fractions, to all 18-helix bundles. We can use these findings in order to lead future investigations of more complex structures that can be assembled in one step.

## Acknowledgments

I would like to begin by thanking my advisor, Dr. Carlos Castro, for providing me with the invaluable opportunity to conduct research in his Nanoengineering and Biodesign Laboratory. He has cultivated a multidisciplinary research group that promotes collaboration and creativity which has greatly impacted my perspective on research in academia. Furthermore, he has allowed me to grow as a researcher and scientist by allowing me to take part in events and conferences, like the Denman, and AICHE, with his full support.

I would like to also thank Joshua Johnson and Dr. Alexander Marras, for mentoring me and teaching me what it takes to be a great researcher. They have continually challenged me throughout my career to promote my own thought process and in the process have become great friends of mine.

My lab partners within NBL, have truly created a wonderful experience for me as they have inspired me with their passions for science and exploration. I have learned a lot from this group of people and have realized that my future lies in research as well. It is due to the influences that I have had through my undergraduate research experience that have propelled me toward pursuing a PhD in chemical engineering. With this degree I hope to lead a multidisciplinary and collaborative group of individuals, in the field of bioengineering to help expand the knowledge of the field.

Finally, I would like to thank my friends and family for their support throughout my undergraduate career. They have been one of the main factors leading to all of my accomplishments.

# Vita

## Education

Ohio State University, Columbus, OH …….. 08/2014 – 05/2018

West Florence High School, Florence, SC……..... 2013-2014

Velo Senior High School, Velo, Greece……..... 2010-2013

## Work Experience

The Ohio State University, Research Assistant, Columbus, OH…… 05/2015 – 05/2018

The Ohio State University, OhioMOD President, Columbus, OH……. 12/2015 – 05/2017

Guild Biosciences, R&D Intern, Dublin, OH……..... 06/2016 - 08/2016

The Ohio State University, Teaching Assistant, Columbus, OH……... 01/2017 – 12/2017

Vantage Oleochemicals, Process Engineer Intern, Chicago, IL……. 05/2017 – 08/2017

## Publications

Marras, A. E., Zhou, L., **Kolliopoulos, V.**, Su, H. J., & Castro, C. E. "Directing folding pathways for multi-component DNA origami nanostructures with complex topology." *New Journal of Physics*, *18*(5), 055005. (2016).

Johnson, J.*, **Kolliopoulos, V.***, Castro, C.E. "Orthogonal Self-assembly of multiple DNA origami nanostructures within a single reaction." (*in preparation*) *equal contributions

## Fields of Study

Major Field: Chemical and Biomolecular Engineering

Table of Contents

Abstract ..... ii
Acknowledgments ..... iii
Vita ..... iv
List of Figures ..... 6
Chapter 1. Introduction ..... 8
Background and Motivation ..... 8
Significance ..... 12
Research Goals ..... 12
Chapter 2. – Methodology ..... 14
Structure Design ..... 14
Individual DNA origami fabrication and characterization ..... 15
Multi-structure fabrication and characterization ..... 16
Equilibrium Folding Study ..... 17
Kinetics Study ..... 19
Characterization via Gel Electrophoresis ..... 20
Characterization via Transmission Electron Microscopy ..... 20
Quantification Method ..... 21
Chapter 3. – Results ..... 22
Individual structure folding ..... 24
Multiple structure folding ..... 27
Chapter 4. – Conclusion ..... 32
Bibliography ..... 33
Appendix A. Other Figures ..... 35
Appendix B. Matlab Code ..... 37

List of Figures

Figure 1: DNA Origami Introduction: DNA origami is fabricated by combining a single stranded DNA molecule (known as scaffold) with hundreds of small strands of DNA (known as staples) which bind to complementary regions to create designed 2D and 3D structures. ..... 8
Figure 2: Survey of DNA origami nanostructures: (A) 2D DNA origami designs courtesy of Rothemund, Nature 2006 [2]. (B) 3D DNA origami designs courtesy of. Marras et al. [11], Hudoba et al. [12], Zhou et al [13]..... 9
Figure 3: This figure has been taken from the following publication [6]. Assembly landscape for multi-component DNA origami slider. ..... 10
Figure 4: Standard origami anneals and the proposed competitive anneal scaffold state [16]. .... 11
Figure 5: (A) Cross section of the 6HB along with a segment of the structures scaffold (blue) and staple (green) routing. (B) Cross section of 18HB along with a segment of the structures scaffold (blue) and staple (black) routing. ..... 15
Figure 6: 18HB (200 nM) sample, characterized using gel electrophoresis. The first lane is the scaffold lane, used as a control, and the following 8 lanes are 18HB samples annealed for 4 hrs at 58° to 52°C. The optimum folding temperature is determined to be around 56°C (boxed in green). When visualized under TEM the resulting structures would appear as depicted below the gel. ..... 16
Figure 7: An equilibrium study of the 40nM 6HB folded with 8 concentrations of 18HB ranging from 0nM to 120nM (left to right). ..... 18
Figure 8: Kinetics study of the 40 nM 6HB. It appears to fold within 5 min with some apparent improvement in yield over the time-scale of several hours to 1 day. ..... 19
Figure 9: Gel electrophoresis depicting a combined fold of 20 nM 6HB and 60 nM 18HB. The first lane is the scaffold control (on left). The 18HB is the leading band (orange arrow) and the 6HB is the lagging band (green arrow). The sample excised is within the red box. ..... 20
Figure 10: The leading band is the 18HB folding region (between orange lines or 18). The middle band is the 6HB folding region (between the green lines, or 6). The rest of the band is the chimera region (between the blue lines, or C). ..... 21
Figure 11: Prismatic Joint [6]. The track is depicted in black and the tube is depicted in grey. .. 22
Figure 12: (a) By removing selected staple crossovers we can control the binding energy of staples, programming track staples to bind before tube staples, therefore folding components in the desired sequence during a standard thermal annealing ramp. (b) A slider where the track forms first (figure S7) shows a lower theoretical binding energy for the track staples and a partial folding ramp reveals the track forming first. (c) The case with unmodified staples (figure S10) shows a similar binding energy for both components and results in misassembled (non-concentric) components. (d) Similarly, the case where the tube folds first (figure S11) also produces misassembled sliders. Scale bars = 50 nm. [6]..... 23
Figure 13: Gel shift assay of isothermal annealing protocol for 6HB structures at 200, 40, 30, and 20 nM staple concentrations (green ramp) and the same annealing protocol for 18HB structures at 200, 120, 80, 40, and 20 nM staple concentrations (yellow ramp). ..... 25

Figure 14: Quantification of folding as a function of folding temperature and concentration for 6HB (A) and 18HB (B) based on the gels displayed in Figure 13. ..... 26
Figure 15: Gel shift assay of 6HB staples at low concentrations with titrations of 18HB staples showing a transition from 6HB folded structures to 18HB folded structures (A). Confirmation via TEM show 6HB structures deposited next to 18HB from excised gel bands (B). ..... 28
Figure 16: Quantified data of combined folding gels repeated in triplicate (left). Phase diagram for the 6HB and 18HB combination folding (right), where red indicated 18HB folding, blue indicated 6HB folding, and in between colors indicate folding of mixtures. ..... 29
Figure 17: Combination fold of 30 nM 6HB and 50 nM 18HB for 8 different time points followed by a 2.5-day control (200 nM) 6HB and 18HB. Chimera region (blue) dissipates in intensity as time increases. The 6HB region increases in intensity with time (green). The 18HB region increases with time (yellow). ..... 30
Figure 18: Comparison of individual versus combination structure kinetics at 30 nM. In an individual reaction the 6HB begins to fold within 30 min (green). In an individual reaction the 18HB begins to fold within 1 hr (yellow). In a combination fold both structures fold between 1 hr and 2 hrs (red). ..... 31
Figure 19: Kinetics study for combination folds. ..... 35
Figure 20: (A) Conceptual folding landscape with the potential for chimera structure proceeding into full folding of one structure or the other. (B) Chimera band noticed. The chimera structures resemble axes. ..... 36

Chapter 1. Introduction

## Background and Motivation

Structural DNA nanotechnology utilizes DNA strands as the building blocks to fabricate nanostructures [1]. DNA origami was pioneered and developed by Dr. Paul Rothemund in 2006 [2] whereby a 7000-8000 base single stranded DNA (ssDNA) loop, referred to as a scaffold, mixed with a set of ~150-200 custom-designed 20-50 base ssDNA segments, termed staples, allowing for the formation of two-dimensional nanostructures. The basic concept is illustrated in Figure 1.

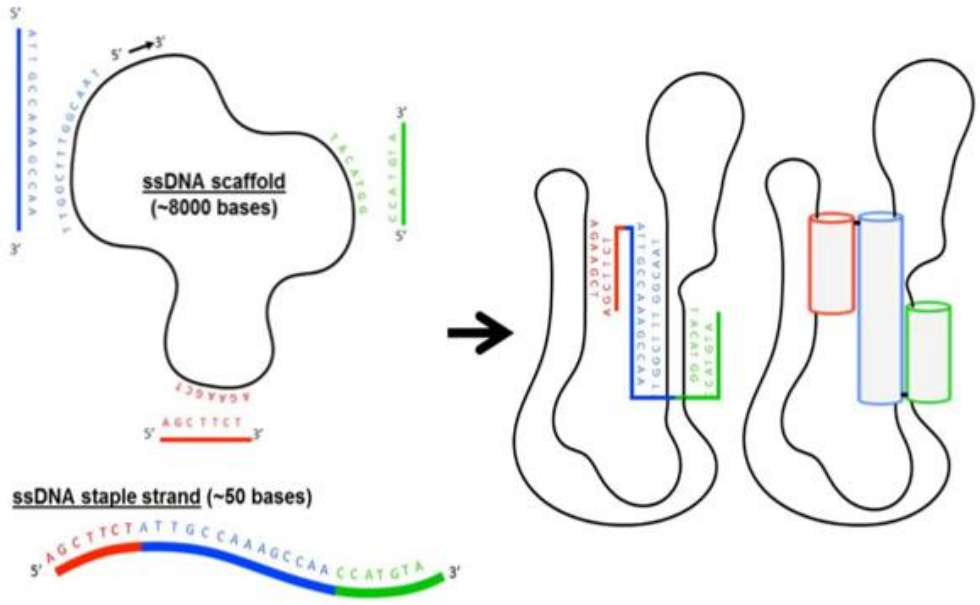


**Figure 1:** DNA Origami Introduction: DNA origami is fabricated by combining a single stranded DNA molecule (known as scaffold) with hundreds of small strands of DNA (known as staples) which bind to complementary regions to create designed 2D and 3D structures.

A multitude of subsequent studies have shown the successful fabrication of three dimensional static and dynamic nanostructures following the same principles, shown in Figure 2

[3] [4] [5] [6], with nanometer geometric precision [2]. Within the past decade, the field of DNA origami has made significant advancements towards several applications including single molecule force measurements [7], fabrication of artificial nanopores [8], and as a drug delivery vehicle [9]. However, a limited number of studies have investigated the intricacies of the DNA origami folding process and, therefore, mechanisms to control, improve, and scale the self-assembly folding process remain poorly understood [10].

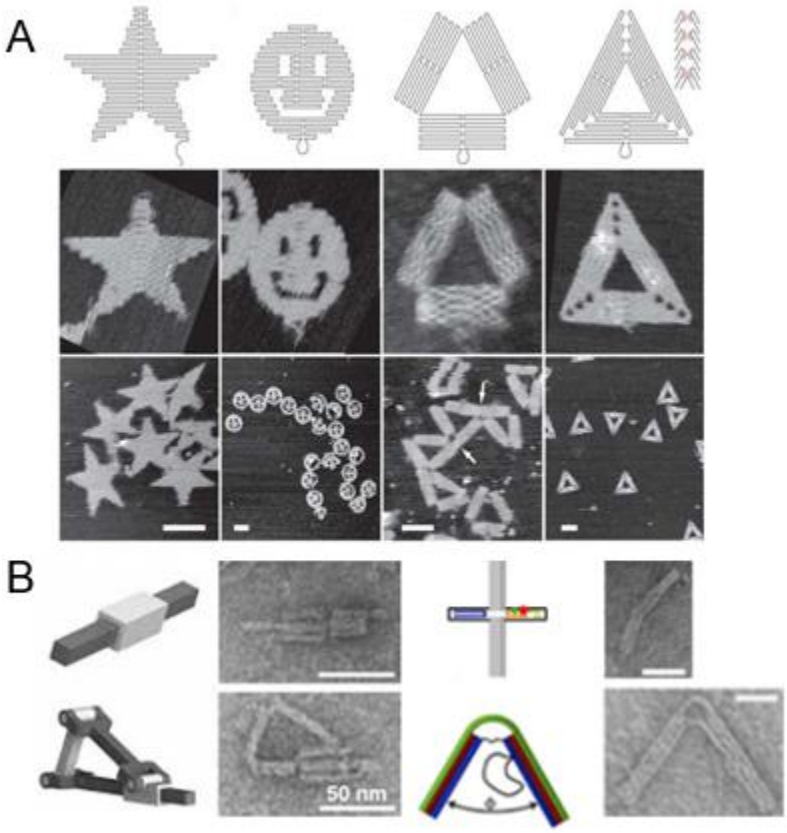


**Figure 2:** Survey of DNA origami nanostructures: (A) 2D DNA origami designs courtesy of Rothemund, Nature 2006 **[2]**. (B) 3D DNA origami designs courtesy of. Marras et al. **[11]**, Hudoba et al. **[12]**, Zhou et al **[13]**.

Controlling the assembly temperature and rate of DNA nanostructure formation is critical to understanding folding dynamics and manufacturing higher order DNA nanostructure assemblies. Staple sequences and length control DNA binding thermodynamics, which can affect overall folding temperatures of DNA origami. Additionally, DNA staple concentrations control the DNA binding kinetics, which is manifested in the rate of folding. Previous findings have reported the domains/components of a single structure can be controlled by both the annealing temperature of the staples and the concentration ratio of staples within that domain [6] [14] [10] [3] [15]. Specifically, a published study [6], where I assisted in data collection and analysis, showed that the order of assembly of segments within a single structure can be controlled by the staple and scaffold design, shown in Figure 3. Thus, this study, demonstrated the ability to control thermodynamic and kinetic factors for individual components in order to optimize the folding of structures that integrate multiple components that fit together with specific topology.

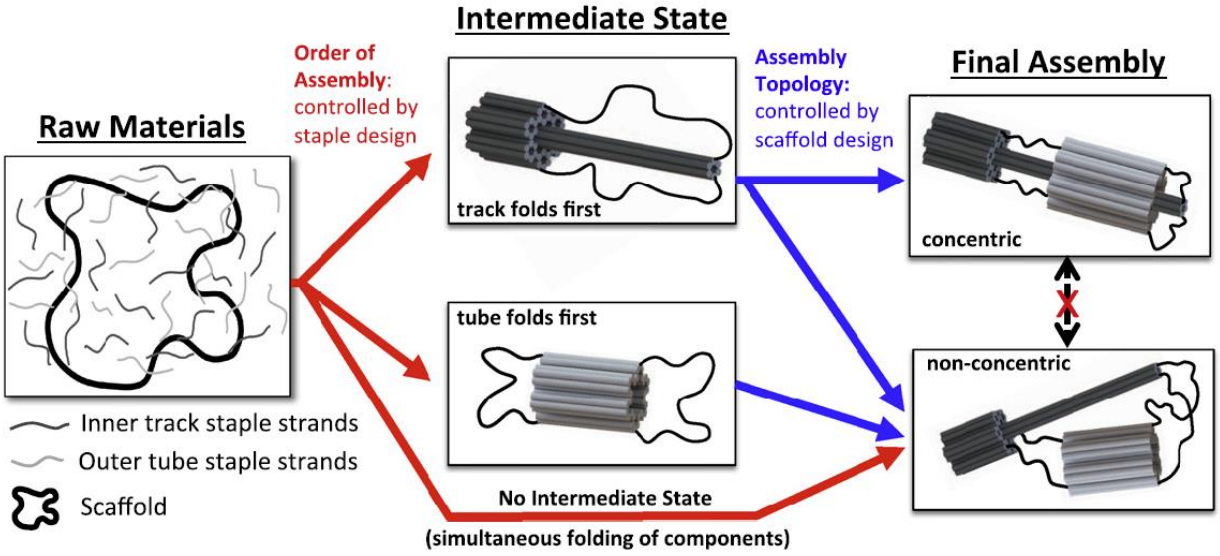


**Figure 3:** This figure has been taken from the following publication **[6]**. Assembly landscape for multi-component DNA origami slider.

A recent published study [16], investigated the simultaneous folding process of systems that contained multiple staple pools for multiple target or parent origami structures. They determined that these simultaneous anneals result in what they named chimeric DNA origami, seen in Figure 4. These chimeric origami structures are a combination of the two parent structures that form due to completion between the parent staple sets. They suggested that competitive anneals of this nature will lead to these chimeric structures providing an interesting was to create diverse nanostructures. In this study, we were inspired by the idea of competitive annealing and focused on creating methods and procedures where the parent structures can successfully fold in high yields in a simultaneous folding reaction.

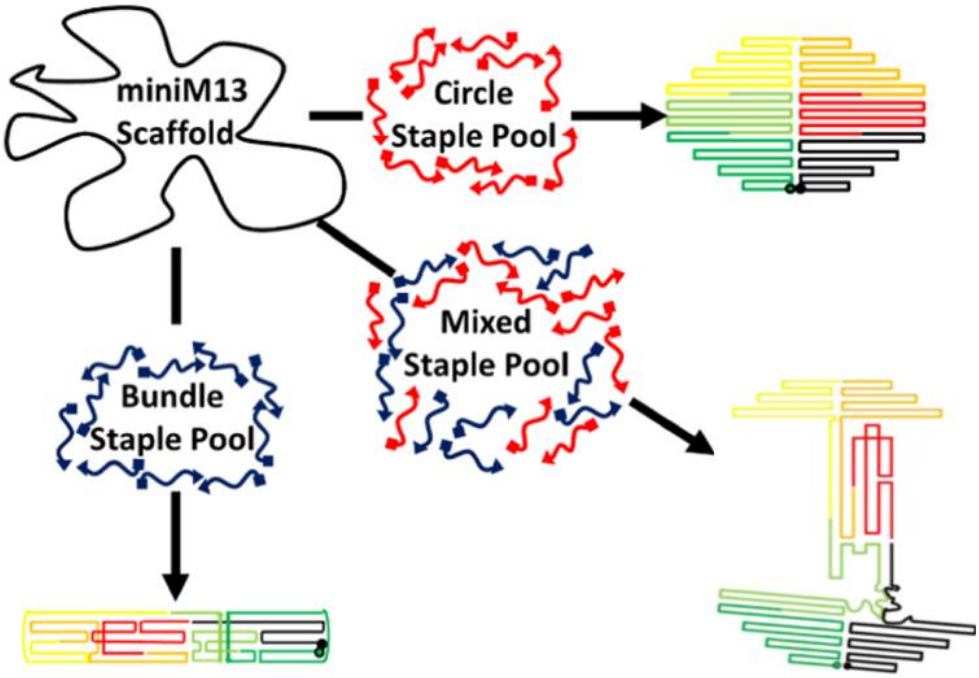


**Figure 4:** Standard origami anneals and the proposed competitive anneal scaffold state **[16]**.

## Significance

Currently, DNA origami molecular self-assembly limits researchers to produce each component separately and connect them to form a higher order nanostructure. This procedure usually results in low yields of the final assembly and is more time consuming. Being able to introduce a standard multi-component one step folding assembly procedure would significantly progress the field by generally improving the efficiency of nanostructure formation, increasing the yield of complex assemblies, and reducing the overall manufacturing costs in terms of time and materials. In addition, a better understanding of the folding dynamics of DNA origami self-assembly and the establishment of improved assembly control strategies can greatly impact the field of DNA origami and biomolecular nanotechnology.

## Research Goals

This project aims to establish robust methods to fold two distinctly different DNA origami structures in one reaction and control the relative yields of each structure. Building on previous research, the effect of varying concentration on the thermodynamics and kinetics of folding will be investigated. Correlations between these fundamental parameters for individual structures will be used to help understand and predict how a mixture of structures will fold. Combinations of structures with varying concentrations will be screened for conditions that successfully fold both structures simultaneously without the formation of undesirable products.

The main research goal is to exploit control over the thermodynamics and kinetics of the DNA origami self-assembly process to optimize folding of a combination of structures and enable control over the relative yield of each structure. We hypothesize that multiple structures

can fold in a single reaction with high overall yield and controllable relative yield by individually controlling the kinetics and thermodynamics of each structure.

# Chapter 2. – Methodology

(The following sections are part of a publication that is in preparation based on joint effort of Joshua Johnson, Dr. Alexander Marras, and myself.)

## Structure Design

DNA origami enables the self-assembly of complex molecular structures due to the programmable nature of DNA. The design of DNA origami nanostructures is facilitated by the open-source design software caDNAno [17]. The design process begins with the hybridization of the long ssDNA scaffold with multiple short ssDNA staples, visualized as bundles in either a honey-comb or square lattice cross section. The caDNAno software presents the user with a two-dimensional schematic of the structure as well as a detailed map of the staples attached to the scaffold along with crossovers that serve as connections between neighboring bundles, shown in Figure 6. Once the staple routing is complete the caDNAno file is exported for verification to a computational tool that uses the finite element method to predict the three-dimensional shape of DNA origami nanostructures, called canDO [15]. For this project, we demonstrate the orthogonal self-assembly of two rod-like structures, a 6-helix bundle (6HB) and 18-helix bundle (18HB) DNA origami nanostructure, shown in Figure 6. These structures were selected from a larger panel of simple rod-like origami design since they annealed in similar folding regions.

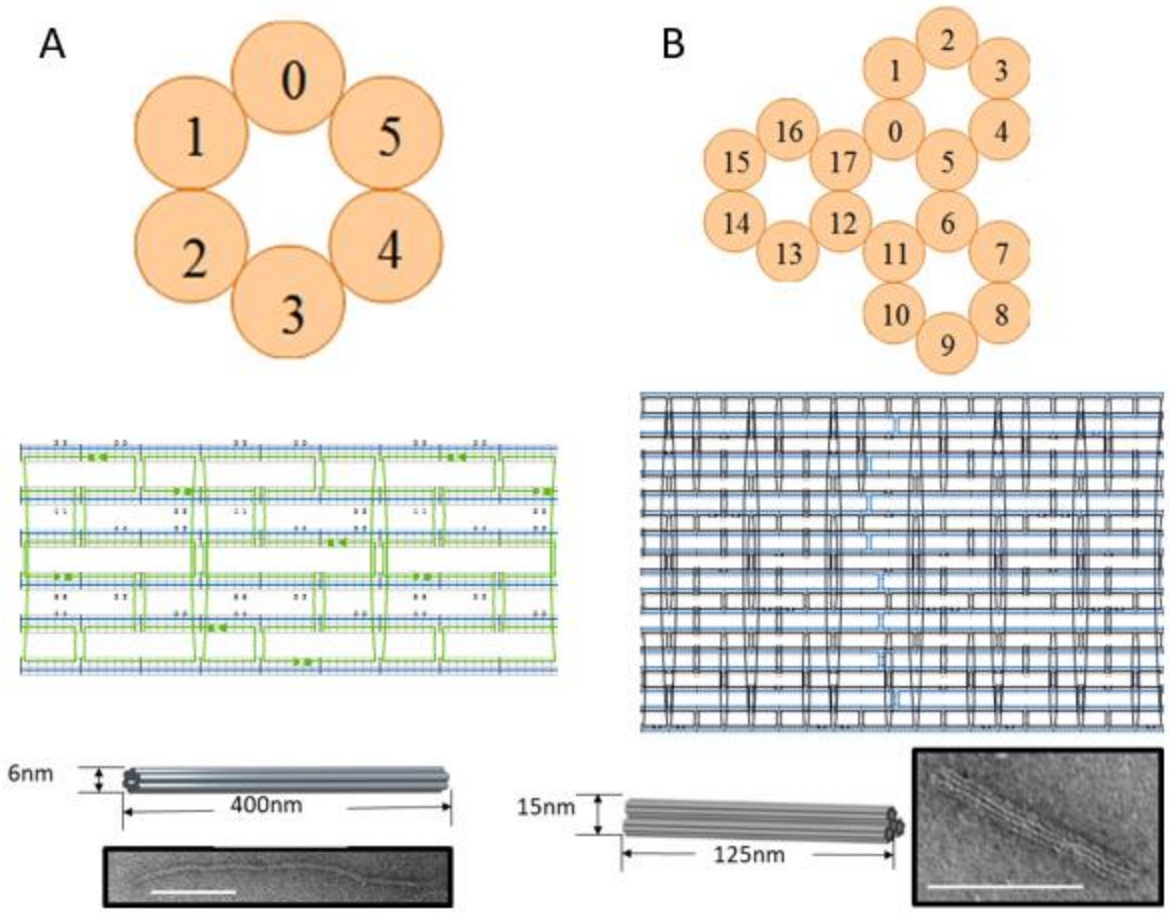


**Figure 5:** (A) Cross section of the 6HB along with a segment of the structures scaffold (blue) and staple (green) routing. (B) Cross section of 18HB along with a segment of the structures scaffold (blue) and staple (black) routing.

**Individual DNA origami fabrication and characterization**

Staples were ordered from commercial vendors while scaffold was produced in house as previously described [15]. A mixture of 20 nM scaffold with a 10-fold excess of staples is prepared in a folding buffer containing 1mM EDTA, 5 mM NaCl, 5 mM Tris, and 18 mM MgCl2. The mixture is aliquoted into an 8-tube strip and subject to a multistep annealing procedure in a thermocycler. First, all tubes are incubated at 65°C for 15 min. Then, a thermal

gradient between 60°C and 40°C is applied for 4 hrs to screen the range of temperatures at which the structure folds. The structures are kept at 4°C until they are evaluated by agarose gel electrophoresis. We define the 'folding temperature' as the maximum temperature which still exhibits a gel shift corresponding to well folded structures. When a rough temperature range is found, the protocol is repeated with a thermal gradient over a smaller range of temperatures to more exactly isolate an upper bound for the folding temperature, see Figure 7. We found that the 6hb folds below ~56°C while the 18hb folds below ~54°C.

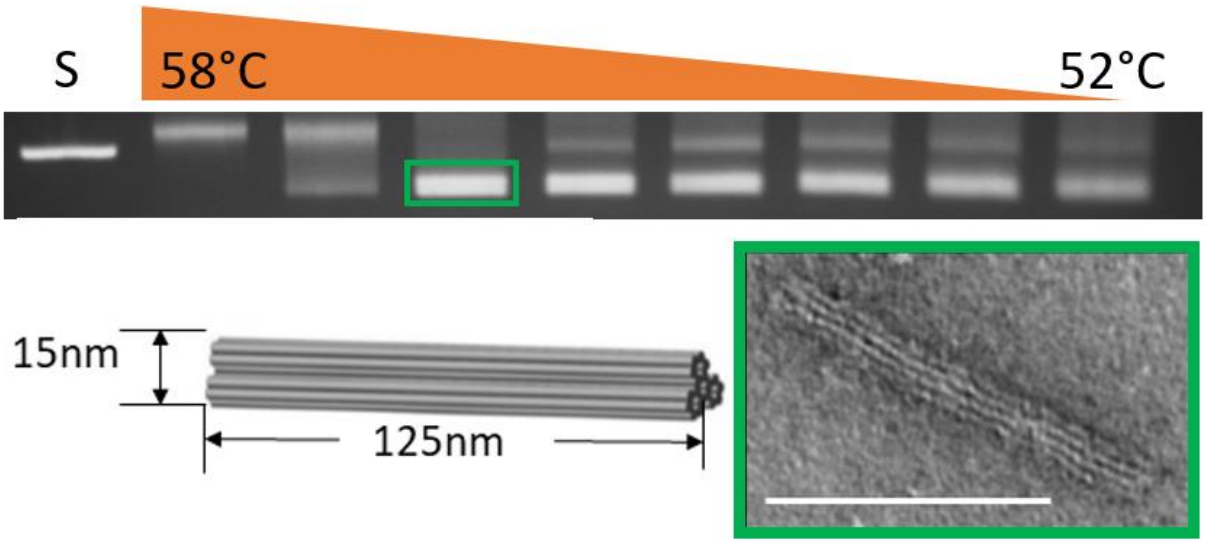


**Figure 6:** 18HB (200 nM) sample, characterized using gel electrophoresis. The first lane is the scaffold lane, used as a control, and the following 8 lanes are 18HB samples annealed for 4 hrs at 58° to 52°C. The optimum folding temperature is determined to be around 56°C (boxed in green). When visualized under TEM the resulting structures would appear as depicted below the gel.

**Multi-structure fabrication and characterization**

To fold multiple structures in a single reaction, a mixture of 20 nM scaffold with a 10-fold excess of staples is prepared in a folding buffer containing 1mM EDTA, 5mM NaCl, 5 mM

Tris, and 18mM MgCl2. The staples in this mixture are a combination of each of the two sets of staples for the two different structures. We tested a range of ratios for the staples from each structure, starting with 50% each. The mixture is aliquoted into an 8-tube strip and subject to a multistep annealing procedure in a thermocycler. The multi-structure folding reaction is characterized as a function of folding temperature to ensure some degree of folding falls within the same ranges as the individual structures. Once the common folding temperature is determined the relative yield of each structure is estimated using an in-house developed Matlab program described in the quantification methods section below.

**Equilibrium Folding Study**

Once we have determined the common folding temperature, where both structures fold in the same reaction, we investigate the thermodynamics of the reaction keeping the folding temperature constant. When folding the combination of two structures in a single reaction with equal staple concentrations, there are three possible outcomes. The first being that neither of the structures fold correctly, the second that both structures fold equally, and finally the third that one structure folds at a higher yield than the other. This study serves to determine methods of better controlling the relative yields of each folded structure type, assuming both structures folded successfully.

The combination fold of the two different structures, at equal staple concentrations, is characterized via gel electrophoresis and TEM. The relative yields of each structure can be determined either by manually counting the structures using transmission electron microscopy (TEM) images, or by using the gel analysis code mentioned in the gel electrophoresis section below. Should one structure fold at higher yields relative to the other, then the higher yield

structure is likely thermodynamically favorable, or the resulting structures are kinetically guided into one configuration. Likely it is both thermodynamics and kinetics that govern the relative yields.

We chose to create a screening procedure to determine how relative concentration of staples affects the folding efficiency of each structure. We selected a concentration for the energetically favorable structure , the 6HB, and kept it constant while we varied the concentration of staples for the less favorable structure, the 18HB. We tested a full factorial design where the energetically favorable structures' staple concentration was 20, 30, or 40 nM while the other structures' staple concentration was 0, 10, 20, 40, 80, 120, 160, or 200 nM, shown in Figure 7.

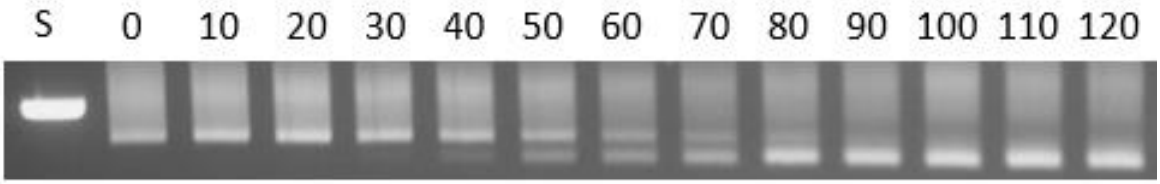


**Figure 7:** An equilibrium study of the 40nM 6HB folded with 8 concentrations of 18HB ranging from 0nM to 120nM (left to right).

A temperature that appears in the common folding region for the two structures is chosen as the common folding temperature. Once this temperature is chosen, the samples undergo a 4-hour isothermal folding protocol and held at the common folding temperature with a 15 min preheat at 65 °C. Finally, the structures are kept at 4°C until they are evaluated by agarose gel electrophoresis. In Figure 7, we notice that at low concentrations of the 18HB we only see a single leading band which falls under the folding region for the 6HB. As we increase the concentration of 18HB we see a second band emerge depicting both structure folding.

**Kinetics Study**

This study serves to investigate the reaction kinetics of the self-assembly process to better understand the folding dynamics of multiple structures in a single reaction. Initially, the folding kinetics of the structures individually were determined. Knowing the folding temperature of each individual structure, we prepared 20, 30, 40, and 200 nM samples of 6HB, aliquoted into an 8-tube strip and folded each concentration at eight different time points (10, 30 min, 1, 2, 4, 8 hrs, 1, 2.5 days). To ensure that no additional folding occurs after a desired time point we arrested the folding by flash freezing samples in liquid nitrogen. The samples were then characterized using gel electrophoresis and visualized using TEM, shown in Figure 8. We repeated the same procedure for the 18HB at 20, 40, 80, 120, 200 nM concentrations each for the 8 different time points.

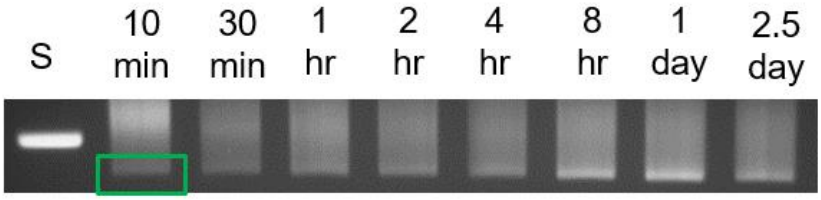


**Figure 8:** Kinetics study of the 40 nM 6HB. It appears to fold within 5 min with some apparent improvement in yield over the time-scale of several hours to 1 day.

Once we characterized the kinetics for each individual structure we proceeded to investigate the kinetics of the two structures in a single reaction. We chose to do this at a 6HB concentration of 30 nM combined with an 18HB concentration of 20, 30, 40, 50, 60, or 70 nM. Using the same procedure as above, samples were made containing the combination of 6HB and 18HB concentrations, aliquoted in 8 tube strips, screened for 8 time points, and flash frozen to arrest the folding. All time points were repeated in triplicate.

**Characterization via Gel Electrophoresis**

Gel electrophoresis was used to verify that the structures folded properly. Mixtures following the annealing protocol were run through a 2% agarose gel in the presence of 0.5X TBE, 11mM $MgCl_2$ and ethidium bromide (EtBr). The gels were run at 90 V for 1-2 hrs for optimal band separation. The resulting gel was imaged on a UV table and the leading bands were excised together as shown in Figure 9.

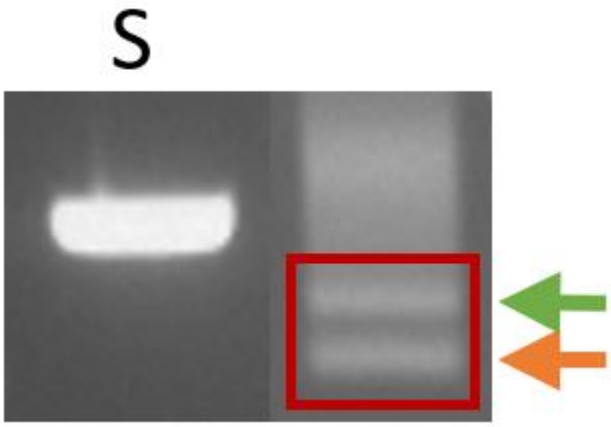


**Figure 9:** Gel electrophoresis depicting a combined fold of 20 nM 6HB and 60 nM 18HB. The first lane is the scaffold control (on left). The 18HB is the leading band (orange arrow) and the 6HB is the lagging band (green arrow). The sample excised is within the red box.

**Characterization via Transmission Electron Microscopy**

Transmission electron microscopy (TEM) was used to further verify and visualize the folded structures. The excised bands from gel electrophoresis were placed in a filter and centrifuged to separate the structures from the gel. The sample was then placed on a copper mesh grid and negatively stained with uranyl formate as previously described [15]. The nanostructures were then imaged under an electron acceleration voltage of 80kV on a Tecnai G2 BioTWIN TEM on the Ohio State University's campus.

**Quantification Method**

A custom Matlab code was used to quantify relative band intensities in agarose gels. For individual folding kinetics two regions of interest are selected which correspond to unfolded structures and fully folded structures. The amount of structure folded is calculated by dividing the sum of pixel intensities in the folded region by the total sum of pixel intensities from both folded and unfolded regions. For combination folding kinetics three regions of interest are selected which correspond to unfolded/chimera structures, folded 18HB, or folded 6HB, shown in Figure 10. Each band intensity is normalized to the total sum of all bands in the lane.

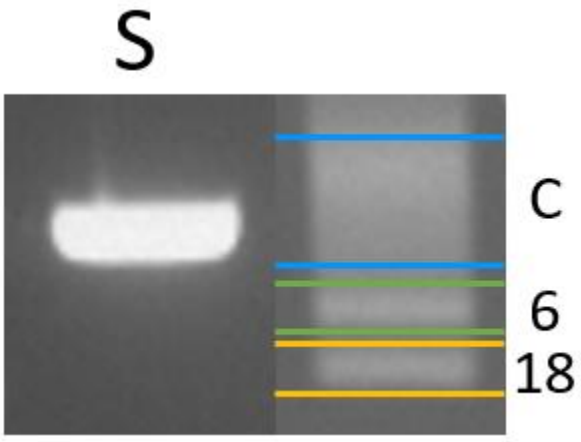


**Figure 10:** The leading band is the 18HB folding region (between orange lines or 18). The middle band is the 6HB folding region (between the green lines, or 6). The rest of the band is the chimera region (between the blue lines, or C).

# Chapter 3. – Results

(The following sections are part of a publication that was a joint effort of Dr. Alexander Marras, Dr. Lifeng Zhou, and myself.)

In a recent publication, that was a collaboration between Dr. Marras and Dr. Zhou and myself, it was shown that one can control the folding pathways for multi-component DNA origami nanostructures by directly controlling the scaffold and staple design [6]. For this publication I assisted in the sample preparation, gel electrophoresis characterization, and manual TEM image counting to quantify percent concentrically and non-concentrically folded structures.

**Figure 11:** Prismatic Joint **[6]**. The track is depicted in black and the tube is depicted in grey.

Dr. Alexander Marras designed a structure, referred to as the prismatic joint, shown in Figure 11, which was comprised of two main components; the track and the tube. We showed that the two components are required to fold in a certain sequence in order to fold concentrically. The track had to fold first and the shell second, as depicted in Figure 12. To do this, we increased the annealing temperature of the staples for the track while we decreased the annealing temperature of the staples for the shell. This way, in an annealing protocol, the track would fold first and the shell would fold second concentric to the track.

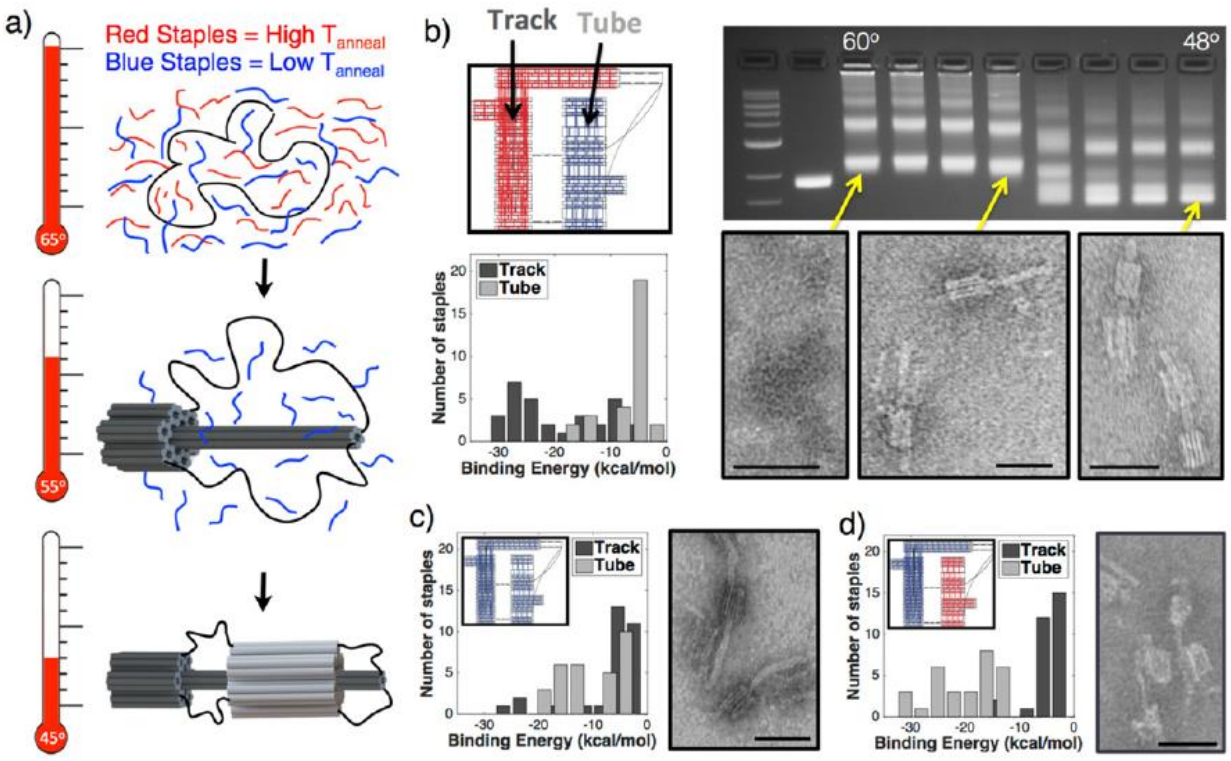


**Figure 12:** (a) By removing selected staple crossovers we can control the binding energy of staples, programming track staples to bind before tube staples, therefore folding components in the desired sequence during a standard thermal annealing ramp. (b) A slider where the track forms first (figure S7) shows a lower theoretical binding energy for the track staples and a partial folding ramp reveals the track forming first. (c) The case with unmodified staples (figure S10) shows a similar binding energy for both components and results in misassembled (non-concentric) components. (d) Similarly, the case where the tube folds first (figure S11) also produces misassembled sliders. Scale bars = 50 nm. **[6]**

This project help inspire the idea of folding multiple structures in a single reaction using similar thermodynamic and design principles. We took on this challenge and using the design principles learned from the project described above we altered the staple annealing temperatures for two staple sets throughout the structures we had chosen, which we called nucleators. When screening these combinations of these nucleated structures, we did not notice a significant effect on their overall annealing temperature so we changed our approach on the topic. We determined

that we would investigate the structure dynamics at their initial designs that had no alteration to the staple segments.

(The following sections are part of a publication that is in preparation based on joint effort of Joshua Johnson, Dr. Alexander Marras, and myself.)

**Individual structure folding**

We initially verified that the 6HB and 18HB could fold in separate reactions at common folding conditions. From gel ESMA electrophortic mobility shift assays, shown in Figure 13, we determined that in an isothermal folding protocol both structures fold in the range of 56°C to 52°C after 4 hours at standard staple concentrations (200nM).

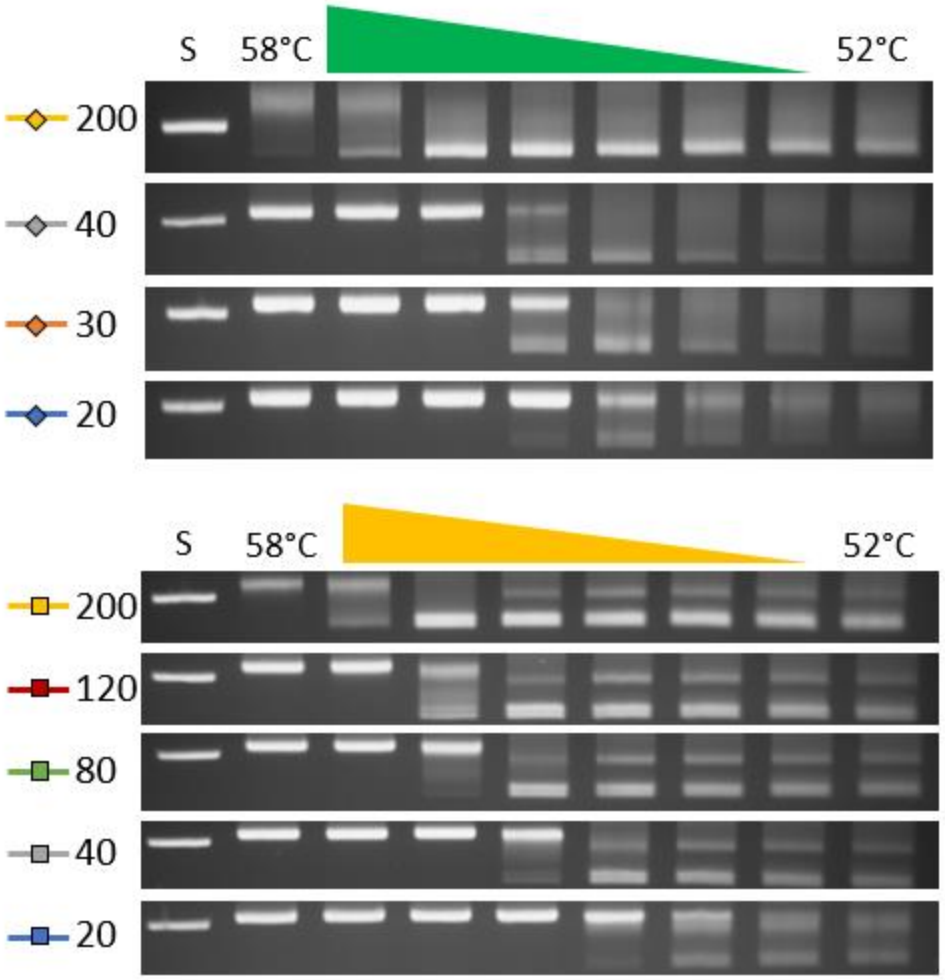


**Figure 13:** Gel shift assay of isothermal annealing protocol for 6HB structures at 200, 40, 30, and 20 nM staple concentrations (green ramp) and the same annealing protocol for 18HB structures at 200, 120, 80, 40, and 20 nM staple concentrations (yellow ramp).

The 18HB structure typically uses a 7249 base pair scaffold but can accommodate a 7560 base pair scaffold while the 6HB structure is only intended for use with a 7560 base pair scaffold. The additional unstructured bases in the 18HB structures are left as an unbound loop of DNA which causes a slight gel shift but otherwise doesn't appear to inhibit folding. At lower staple concentrations, there was a marked decrease in the upper bound of temperatures at which

structures folded. Additionally, the 6HB structure appeared to have reduced yields at below 54°C at staples concentration equal to scaffold concentrations (20 nM), seen in Figure 14. Thus, the overall thermodynamics of folding appear to be more easily controlled in isothermal folding reactions with varying concentrations.

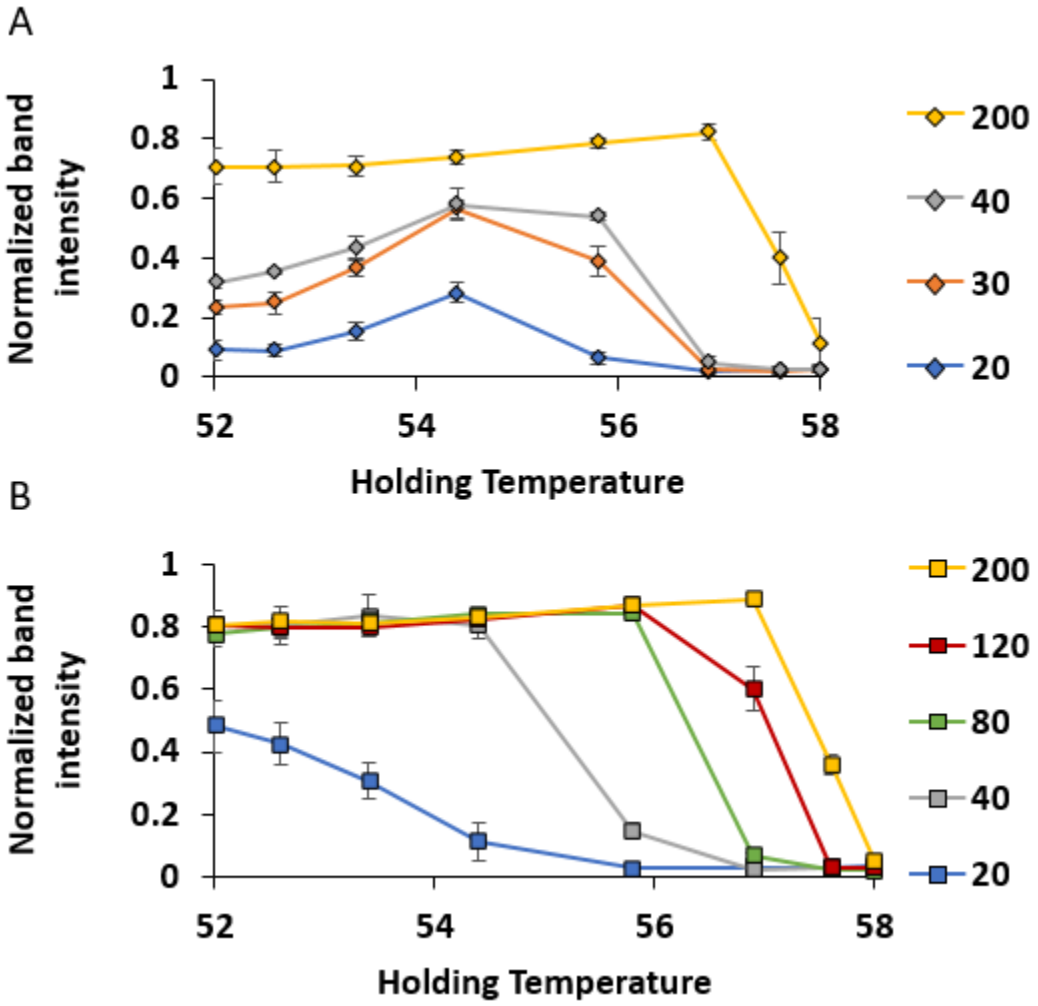


**Figure 14:** Quantification of folding as a function of folding temperature and concentration for 6HB (A) and 18HB (B) based on the gels displayed in Figure 13.

Based on this data we would expect that the 18HB structure would be more likely to fold to completion in a mixed reaction containing equal staples from both structures. Given the large

parameter space available to explore with two origami structures and a custom folding protocol, we chose to proceed with all further folding reactions at the same folding temperature (52.6°C) while only vary the concentration of full staple sets.

**Multiple structure folding**

We then conducted experiments with combinations of staples from 6HB and 18HB structures. We found that the 6HB dominated in the folding reaction when mixed with 18HB staples in an equal ratio. This is still a critical result because it demonstrates that a DNA origami nanostructure can successfully fold in a mixture of interfering strands. We then iterated over several conditions with low concentrations of 6HB (20 to 40 nM) and a full range of 18HB concentrations from 0 to 200 nM shown in Figure 15. From gel shift assays and TEM images, we found that when 18HB staples are approximately 1.5x the concentration of 6HB staples, then both structures successfully self-assemble at approximately equal yields.

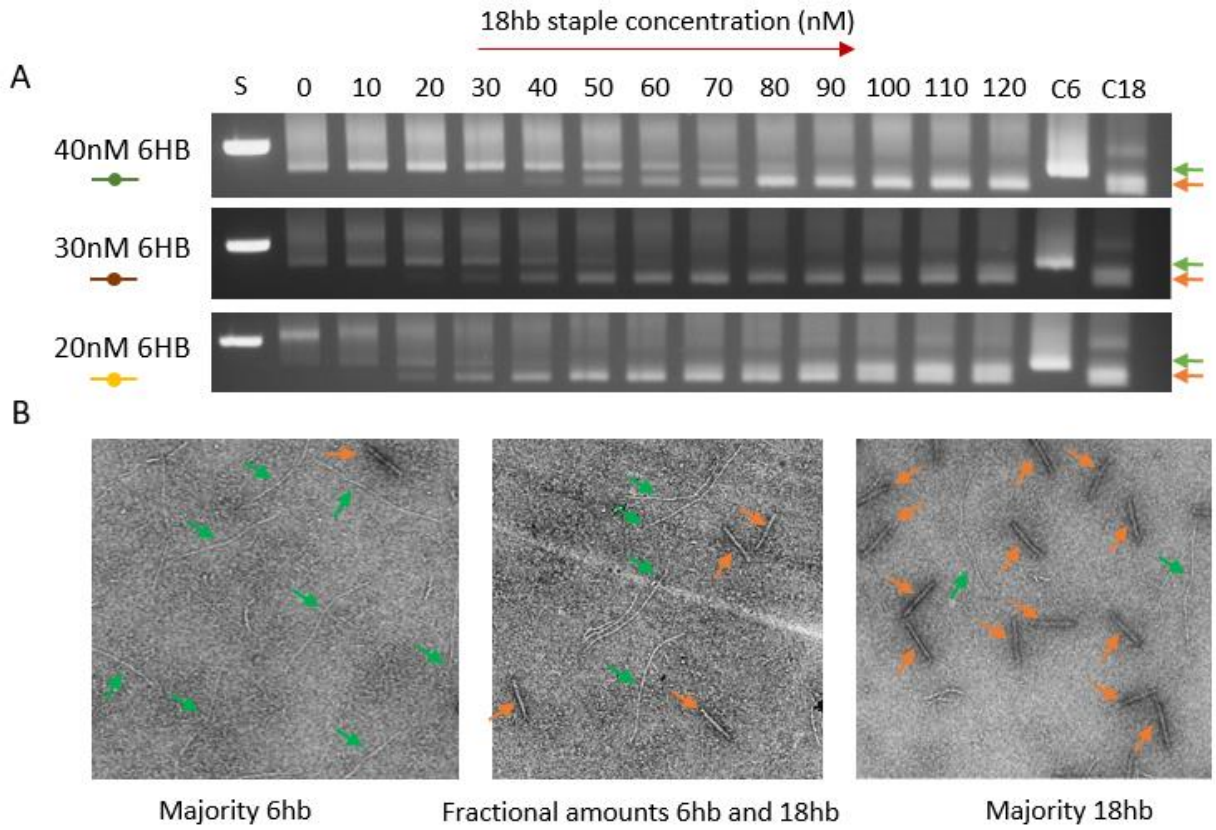


**Figure 15:** Gel shift assay of 6HB staples at low concentrations with titrations of 18HB staples showing a transition from 6HB folded structures to 18HB folded structures (A). Confirmation via TEM show 6HB structures deposited next to 18HB from excised gel bands (B).

With this data we can map out a phase diagram to demonstrate conditions which primarily produce 18HB, 6HB, or a mixture of both, shown in Figure 16. To our knowledge this type of result has not been published before and clearly demonstrates that, even without optimizing staple routings, it is possible to fold two distinct DNA origami nanostructures in desired quantities by simply varying staple concentrations.

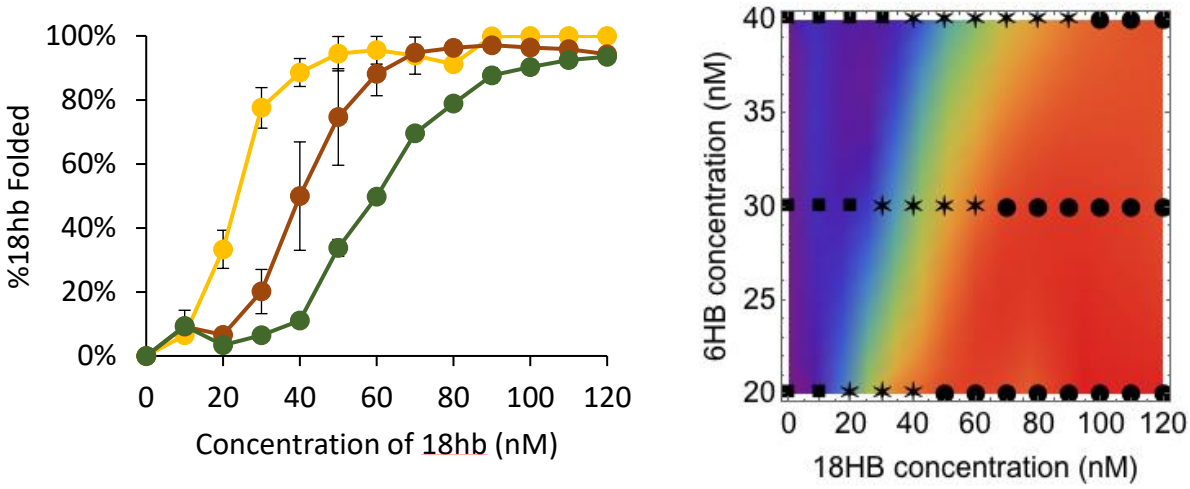


**Figure 16:** Quantified data of combined folding gels repeated in triplicate (left). Phase diagram for the 6HB and 18HB combination folding (right), where red indicated 18HB folding, blue indicated 6HB folding, and in between colors indicate folding of mixtures.

We then looked at the kinetics of folding with multiple staple sets. We arrested folding reactions via cryo-quenching and observed the evolution of structures with gel shift assays and TEM. We tested the kinetics of combination folds for a small range of 18HB and fixed concentration of 6HB, shown in Appendix A Figure 19. At early folding times (within 10 min), partially formed structures appear, sometimes with multiple folded domains. After about an hour of incubation new bands in the gel can be seen corresponding to complete 6HB or 18HB structures, seen in Figure 17. Chimera structures also become better defined as the initially nucleated regions from two different structures have grown to a point where competing domains come in contact with one another. Over longer time periods (up to 60 hrs), the chimera band slowly broadens and dissipates, shown in Appendix A Figure 20. The amount of aggregated matter in the wells increases and there is some increased intensity of folded structure. This seems

to indicate that the chimeras are metastable and eventually convert to either the 6HB or 18HB structures or simply form greater aggregates.

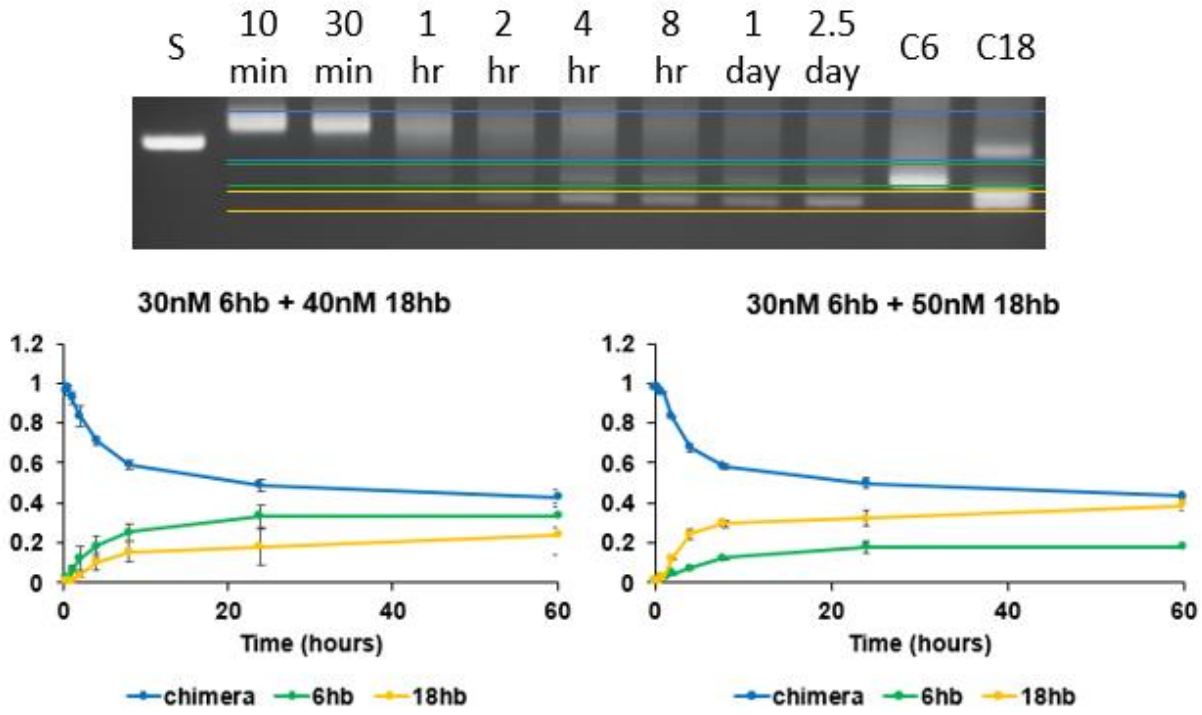


**Figure 17:** Combination fold of 30 nM 6HB and 50 nM 18HB for 8 different time points followed by a 2.5-day control (200 nM) 6HB and 18HB. Chimera region (blue) dissipates in intensity as time increases. The 6HB region increases in intensity with time (green). The 18HB region increases with time (yellow).

The kinetics of a combination fold are much slower than kinetics of individual folds at similar concentrations, see Figure 18. Also, we noted that regardless of concentration the initial folding rates of each structure within a combination fold were very similar. This would again support the idea that only a few initial nucleation events determine the final structure and while folding is slightly impeded by competing interactions the cooperativity between a few initially bound staples facilitates folding to completion.

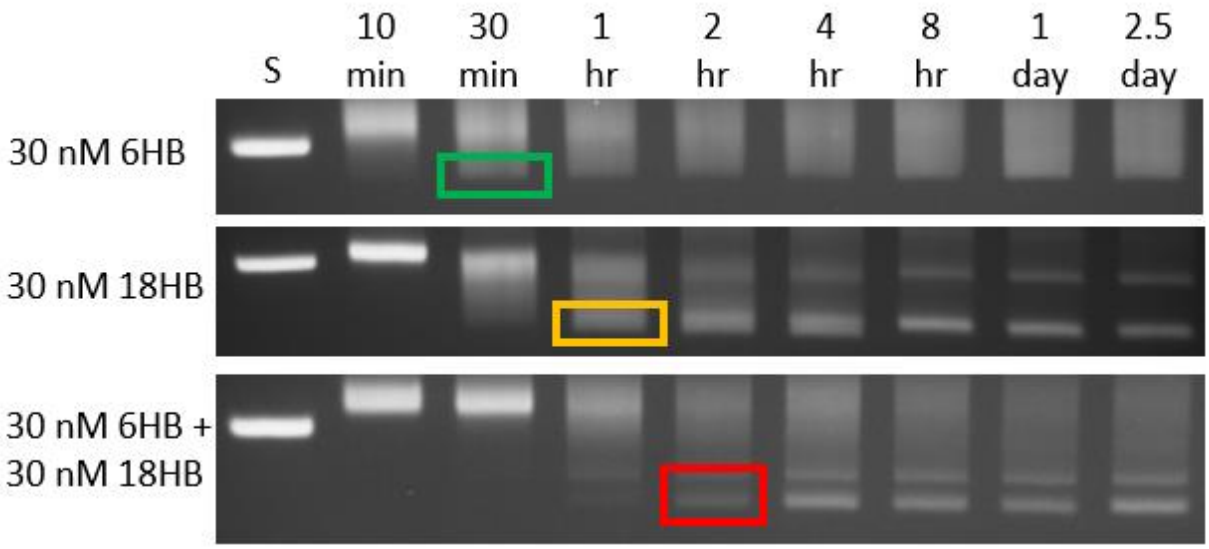


**Figure 18:** Comparison of individual versus combination structure kinetics at 30 nM. In an individual reaction the 6HB begins to fold within 30 min (green). In an individual reaction the 18HB begins to fold within 1 hr (yellow). In a combination fold both structures fold between 1 hr and 2 hrs (red).

# Chapter 4. – Conclusion

Recent research within DNA origami has focused on the investigation and understanding of the self-assembly process that can lead to the ability of controlling the folding process. This thesis presents an innovative and novel method to determine the folding characteristics of the structures of interest. Furthermore, through this understanding, it provides procedures that can lead to the successful fabrication of multiple structures in a single reaction.

We expect that our methods and procedures will impact the field of DNA origami directly, as we provide means for the fabrication of multi-component higher order structures in a single step reaction. This effort opens the possibility for the achievement of unprecedented structure designs with novel applications to the field.

The results presented here are promising for multi-component fabrication, but DNA origami still has limitations to overcome. We will need to investigate the dynamics of complex structure designs identify the underlying principles regardless the geometric constraints. Ongoing research is propelling this effort and our contribution to DNA origami with this fundamental idea will accelerate this understanding.

Bibliography


[1] N. C. Seeman, "Nucleic acid junctions and lattices," *Journal of theoretical biology,* pp. 237-247, 1982.

[2] P. W. Rothemund, "Folding DNA to create nanoscale shapes and patterns.," *Nature,* vol. 440, pp. 297-302, 2006.

[3] S. M. Douglas, H. Dietz, T. Liedl, B. Hogberg, F. Graf and W. M. Shih, "Self-assembly of DNA into Nanoscale Three-dimensional Shapes.," *Nature,* vol. 459, p. 414−418, 2009.

[4] H. Dietz, S. M. Douglas and W. M. Shih, " Folding DNA into Twisted and Curved Nanoscale Shapes.," *Science,* vol. 325, p. 725, 2009.

[5] E. S. Andersen, M. Dong, M. M. Nielsen, K. Jahn, R. Subramani, W. Mamdouh, M. M. Golas, B. Sander, H. Stark, C. L. P. Oliveira, J. S. Pedersen, V. Birkedal, F. Besenbacher, K. V. Gothelf and J. Kjems, "Self-assembly of a Nanoscale DNA Box wit," *Nature,* vol. 459, pp. 73-76, 2009.

[6] A. E. L. Z. V. K. H. J. S. a. C. E. C. Marras, "Directing folding pathways for multi-component DNA origami nanostructures with complex topology," *New Journal of Physics,* vol. 18, no. 5, p. 055005, 2016.

[7] E. Pfitzner, C. Wachauf, F. Kilchherr, B. Pelz, W. M. Shih, M. Rief and H. Dietz, "Rigid DNA Beams for High-Resolution Single- Molecule Mechanics.," *Angew. Chem.,* vol. 52, p. 7766−7771, 2013.

[8] M. Langecker, V. Arnaut, T. G. Martin, J. List, S. Renner, M. Mayer, H. Dietz and F. C. Simmel, "Synthetic Lipid Membrane Channels Formed by Designed DNA Nanostructures.," *Science,* vol. 338, pp. 932-936, 2012.

[9] P. D. e. a. Halley, "DNA Origami: Daunorubicin-Loaded DNA Origami Nanostructures Circumvent Drug-Resistance Mechanisms in a Leukemia Model," *Small,* vol. 12.3, pp. 307-309, 2016.

[10] F. e. a. Dannenberg, "Modelling DNA origami self-assembly at the domain level.," *The Journal of chemical physics,* vol. 143.16 , 2015.

[11] A. E. L. Z. H.-J. S. a. C. E. C. Marras, "Programmable motion of DNA origami mechanisms.," *Proceedings of the National Academy of Sciences,* vol. 112, no. 3, pp. 713-718, 2015.

[12] M. W. Y. L. A. Z. M. G. P. a. C. E. C. Hudoba, "Dynamic DNA Origami Device for Measuring Compressive Depletion Forces.," *ACS nano,* vol. 11, no. 7, pp. 6566-6573, 2017.

[13] L. A. E. M. H.-J. S. a. C. E. C. Zhou, "DNA origami compliant nanostructures with tunable mechanical properties.," *ACS nano,* vol. 8, no. 1, pp. 27-34, 2013.

[14] K. E. e. a. Dunn, "Guiding the folding pathway of DNA origami.," *Nature,* 2015.

[15] C. E. e. a. Castro, "A primer to scaffolded DNA origami.," *Nature methods,* vol. 8.3, pp. 221-229, 2011.

[16] J. M. J. A. N. a. T. H. L. Majikes, "Competitive annealing of multiple DNA origami: formation of chimeric origami," *New Journal of Physics,* vol. 18, no. 11, p. 115001, 2016.

[17] A. H. M. S. T. A. V. G. M. C. a. W. M. S. S. M. Douglas, "Rapid prototyping of 3D DNA-origami shapes with caDNAno.," *Nucleic Acids Research,* pp. 5001-5006, 2009.

[18] J. e. a. Lee Tin Wah, "Observing and Controlling the Folding Pathway of DNA Origami at the Nanoscale.," *ACS nano,* vol. 10.2, pp. 1978-1987, 2016.

[19] X. J. N. a. Y. L. Wei, "Uncovering the self-assembly of DNA nanostructures by thermodynamics and kinetics.," *Accounts of chemical research,* vol. 47.6, pp. 1861-1870, 2014.

[20] D. A. E. M. J. L. C.-M. H. L. Z. C. E. C. H.-J. S. a. G. R. Lei, "Three-dimensional structural dynamics of DNA origami Bennett linkages using individual-particle electron tomography.," *Nature communications,* vol. 9, no. 1, p. 592, 2018.

Appendix A. Other Figures

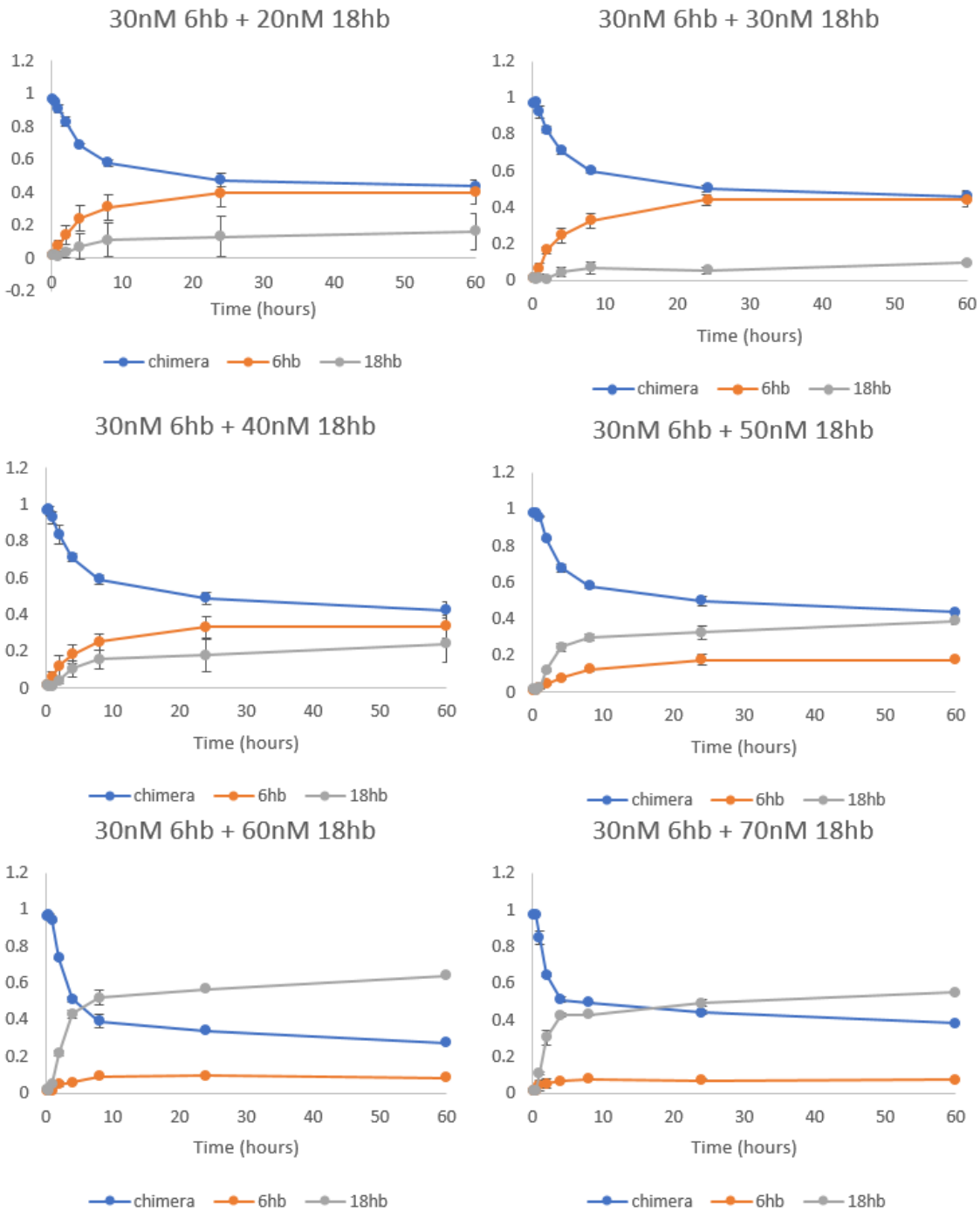


**Figure 19:** Kinetics study for combination folds.

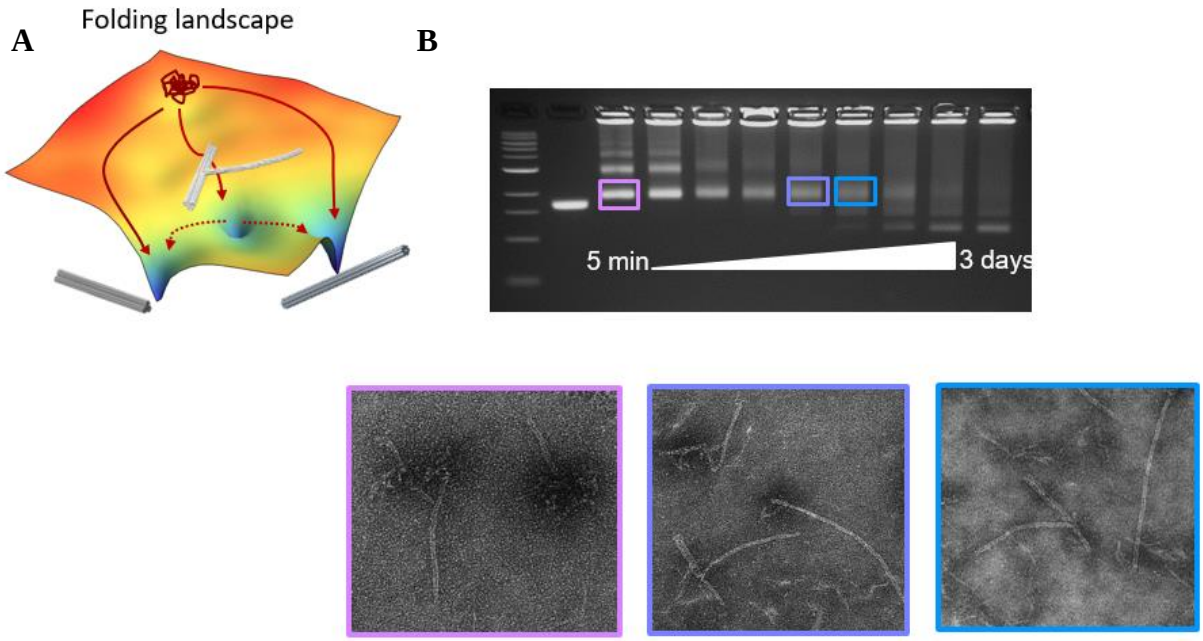


**Figure 20:** (A) Conceptual folding landscape with the potential for chimera structure proceeding into full folding of one structure or the other. (B) Chimera band noticed. The chimera structures resemble axes.

# Appendix B. Matlab Code

```
% Gel Analysis Two-Zones
% plotting and quantifying gel images rapid fold and kinetics

clc, clear all, close all

N = 8; % number of bands EXCLUDING SCAFFOLD AND LADDER
autorotate = 0;
[filename pathname]=uigetfile('.tif');
gel_gray = imread(strcat(pathname, filename));
%gel_gray = imread('160403(Hin S4 R234 9nt + 5xAuNP + buffer DNA).tif');
% gel_gray = imread('2015-08-21 20nM 2hb + 0-200nM 18hb 1 and 2 repeats +
40nM 6hb +0-200nM 18hb 1 and 2 repeats at 52p6deg 4hr rf.tif');
gel_double = padarray(im2double(gel_gray(:,:,1)),[15 15]);
rect0 = [135.5100    0.5100  488.9800  103.9800];
h1 = figure(1);
imshow(gel_double)
xlabel('crop image INCLUDING Scaffold and
ladder','FontSize',20,'Fontweight','bold')
gel_crop_rect = imrect(gca, rect0);
pause
rect = gel_crop_rect.getPosition;
xpos = rect(1);
ypos = rect(2);
box_width = rect(3);
box_height = rect(4);

gel_crop_im = gel_double(ypos:(ypos+box_height),xpos:(xpos+box_width));
I = imresize(im2double(gel_crop_im),2,'bicubic');
figure(1);
imshow(I)
profile = sum(I,1);
Y=fft(profile);
Y(1)=[];
% plot(Y,'ro')
n = length(Y);
power = abs(Y(1:floor(n/2))).^2;
nyquist = 1/2;
freq = (1:n/2)/(n/2)*nyquist;
period = 1./freq;
% figure(2)
% plot(period,power)
% % axis([0 200 0 inf]);
% xlabel('cycles/pixel')
% title('Periodogram')
index = find(power(5:end) == max(power(5:end)))+5;
lane_width = period(index)
%% Background subtract
filterEl=strel('rectangle',[round(1.5*lane_width), 2*round(lane_width)]);
background = imgaussfilt(imopen(I,filterEl),lane_width/16);
[r, c] = size(I);
gel_norm = medfilt2(I - background,[4 4]);
```

```
figure(1), imshow(gel_norm,[]),colormap jet
% figure(2), imshow(background,[])
% pause
%% Autorotate
if autorotate == 1
    pad = round(0.1*size(I,1));
    I_pad = padarray(gel_norm,[pad pad],'replicate');
    best_rot = I;
    best_pksum =0;
    for i=-5:0.2:5
        I_rot = imrotate(I_pad,i,'crop');
        I_crop = I_rot(pad:size(I,1)+pad,pad:size(I,2)+pad);

        profile = sum(I_crop,1);
        sm = smooth(profile,lane_width/5);
        deriv = smooth(abs(diff(sm)),9);
        deriv(1:4) = 0;
        d_tot = sum(deriv);
        d_norm = deriv./d_tot;
        [maxpk, maxind] = findpeaks(d_norm,'Threshold',0.0002);
        figure(2)
        findpeaks(d_norm,'Threshold',0.0002)
        plot(deriv)
        maxpk(1) = 0;
        pksum=sum(maxpk);
        if pksum>best_pksum
            best_pksum = pksum;
            best_rot = I_crop;
        end
    end
    figure(2), imshow(best_rot,[]),colormap jet;
end
%% Manual rotate
if autorotate == 0
    pad = round(0.1*size(I,1));
    I_pad = padarray(gel_norm,[pad pad],'replicate');
    figure(2)
    imshow(I,[])
    colormap jet
    xlabel('Set line for rotation','FontSize',20,'Fontweight','bold')
    rot_line = imline(gca);
    pause
    rot_pos = rot_line.getPosition;
    rot_x1 = rot_pos(1,1);
    rot_x2 = rot_pos(2,1);
    rot_y1 = rot_pos(1,2);
    rot_y2 = rot_pos(2,2);
    theta_rot = 180/pi*atan((rot_y2-rot_y1)/(rot_x2-rot_x1));

    I_rot = imrotate(I_pad,theta_rot,'crop');
    best_rot = I_rot(pad:size(I,1)+pad,pad:size(I,2)+pad);
    profile = sum(best_rot,1);
    sm = smooth(profile,lane_width/5);
end
```

```
%
%% Lane detection
r1=size(best_rot,1);
c1=size(best_rot,2);
deriv = smooth(diff(sm),5);
deriv(1:5)=0;
[maxpk, maxind] = findpeaks(deriv,'MinPeakDistance',round(0.9*lane_width));
[minpk, minind] = findpeaks(-deriv,'MinPeakDistance',round(0.9*lane_width));
%
% figure(2)
% imshow(best_rot,[]), colormap jet
% figure(3)
% hold on
% findpeaks(deriv,'MinPeakDistance',round(0.9*lane_width));
% findpeaks(-deriv,'MinPeakDistance',round(0.9*lane_width));
if minind(1)<lane_width/2
    minind = minind(2:end);
end
if maxind(end)>(c1-0.8*lane_width)
    maxind = maxind(1:end-1);
end

% for i=1:size(maxind,1)
%     plot(maxind(i)*ones(1,r1),1:r1,'g','linewidth',2)
%     plot(minind(i)*ones(1,r1),1:r1,'r','linewidth',2)
% end
%% Advanced background subtractions
ypts = 5:round(lane_width/2):r1;
midlane = round((minind+maxind)/2 + lane_width/2);
midlanex = zeros(size(midlane,1)*size(ypts,1),1);
midlaney = zeros(size(midlane,1)*size(ypts,1),1);
midlanez=zeros(size(midlane,1)*size(ypts,1),1);
for j=1:size(midlane,1)
    for k=1:size(ypts,2)
        ind = (j-1)*size(ypts,2)+k;
        midlanex(ind) = midlane(j);
        midlaney(ind) = ypts(k);
        midlanez(ind) = best_rot(midlaney(ind), midlanex(ind));
%         figure(2),ho ld on
%         plot(midlanex(ind),midlaney(ind),'kx','Linewidth',2,'MarkerSize',10
)
    end
end
poly3 = polyfitn([midlanex midlaney],midlanez,3);
[r, c] = size(best_rot);

[x_grid, y_grid] = meshgrid(1:c,1:r);
x_bg1 = reshape(x_grid,r*c,1);
y_bg1 = reshape(y_grid,r*c,1);
z_bg1 = polyvaln(poly3,[x_bg1 y_bg1]);

x_bg = reshape(x_bg1,r,c);
y_bg = reshape(y_bg1,r,c);
z_bg = reshape(z_bg1,r,c);
```

```
% figure(3)
%
surf(best_rot,'EdgeColor','none','FaceLighting','gouraud','EdgeLighting','gou
raud')
% view([0 1 0.5])
% set(gcf,'Position',[450 25 400 400])
% x_lim = get(gca,'Xlim');
% y_lim = get(gca,'Ylim');
% z_lim = get(gca,'Zlim');
% xlabel('Pre background subtration','FontSize',20,'Fontweight','bold')
% set(gca,'Clim',[min(min(gel_crop_im)) max(max(gel_crop_im))])

% figure(4)
%
surf(z_bg,'EdgeColor','none','FaceLighting','gouraud','EdgeLighting','gouraud
')
% view([0 1 0.5])
% set(gcf,'Position',[875 25 400 400])
% set(gca,'Xlim',x_lim,'Ylim',y_lim,'Zlim',z_lim)
% xlabel('Fitted background','FontSize',20,'Fontweight','bold')
% set(gca,'Clim',[min(min(gel_crop_im)) max(max(gel_crop_im))])

gel_norm = best_rot - z_bg;
figure(2)
imshow(gel_norm,[]),colormap jet,hold on
for i=1:size(maxind,1)
    plot(maxind(i)*ones(1,r1),1:r1,'g','linewidth',2)
    plot(minind(i)*ones(1,r1),1:r1,'r','linewidth',2)
end
% figure(5)
%
surf(gel_norm,'EdgeColor','none','FaceLighting','gouraud','EdgeLighting','gou
raud')
% view([0 1 0.5])
% set(gcf,'Position',[1300 25 400 400])
% xlabel('Post background subtraction','FontSize',20,'Fontweight','bold')
%% Select folded regions
figure(2)
xlabel('Set top of 1st folded band region','FontSize',20,'Fontweight','bold')
h_line1 = imline(gca);
pause
pos_line1 = h_line1.getPosition;
c1 = polyfit(pos_line1(:,1)',pos_line1(:,2)',1);

pos_line2 = pos_line1;
pos_line2(:,2) = pos_line2(:,2)+14;
xlabel('Set bottom of 1st folded band
region','FontSize',20,'Fontweight','bold')
h_line2 = imline(gca,pos_line2);
pause
pos_line2 = h_line2.getPosition;
c2 = polyfit(pos_line2(:,1)',pos_line2(:,2)',1);
```

```
pos_line3 = pos_line2;
xlabel('Set top of 2nd folded band region','FontSize',20,'Fontweight','bold')
h_line3 = imline(gca,pos_line3);
pause
pos_line3 = h_line3.getPosition;
c3 = polyfit(pos_line3(:,1)',pos_line3(:,2)',1);

pos_line4 = pos_line3;
pos_line4(:,2) = pos_line4(:,2)+14;
xlabel('Set bottom of 2nd folded band
region','FontSize',20,'Fontweight','bold')
h_line4 = imline(gca,pos_line4);
pause
pos_line4 = h_line4.getPosition;
c4 = polyfit(pos_line4(:,1)',pos_line4(:,2)',1);

%%
band_left = maxind(3:size(maxind,1));
band_right = minind(3:size(minind,1));
% summing intensity in folded structure band for each lane
band_sum1 = ones(1,N);
band_sum2 = ones(1,N);
profiles = zeros(r1,N);

for i=1:N
    y1_top = round(c1(1)*band_left(i)+c1(2));
    y1_bot = round(c2(1)*band_left(i)+c2(2));
    y2_top = round(c3(1)*band_right(i)+c3(2));
    y2_bot = round(c4(1)*band_right(i)+c4(2));

    band_im = best_rot(:,(band_left(i)):(band_right(i)));
    sb = strel('rectangle',[(y2_bot-y1_top)*2,round(size(band_im,2)*.6)]);
    band_back=imopen(band_im,sb);
    profiles(:,i) = sum(band_im-band_back,2);
    band_width = band_right(i)-band_left(i);
    band_sum1(:,i) = sum(profiles(y1_top:y1_bot,i));
    band_sum2(:,i) = sum(profiles(y2_top:y2_bot,i));


end
%%
lane = 1:N;

% Change the independent variable to the appropriate time or temperature
series
Temp = fliplr([40 41.7 44.4 47.8 52.5 56 58.4 60]);
% Temp = fliplr([48 48.4 48.9 49.6 50.5 51.2 51.7 52]); % LPP fine screen
% Temp = fliplr([50.0 50.4 50.9 51.6 52.5  53.2 53.7 54.0]); % 18hb fine
screen
Conc = [0 10 20 30 40 50 60 70 80 90 100 110 120];
% Time = [1 2 3 4 5 10 15];
Time = [1/6 .5 1 2 4 8 24 60];
% band_sum1 = sum(y1_fit)./sum(profiles);
% band_sum2 = sum(y2_fit)./sum(profiles);
```

```
tot_band_int = sum(profiles);

band_sum_norm1 = band_sum1./tot_band_int;
band_sum_norm2 = band_sum2./tot_band_int;

xplot = Time;

% figure(13),hold on, box on
% set(gcf,'Color',[1 1 1])
% set(gca,'FontSize',30,'Xlim',[min(xplot)
max(xplot)],'Xdir','normal','Ylim',[-10 180])
% % set(gca,'FontSize',30,'Xlim',[min(Time) max(Time)],'Ylim',[-10 320])
% plot(xplot,band_sum1,'r','linewidth',2)
% plot(xplot,band_sum2,'k','linewidth',2)
% % plot(Time,band_sum,'k','linewidth',2)
% % xlabel('Annealing Temperature (^oC)','FontSize',30)
% xlabel('Concentration of 18hb (nM)','FontSize',30)
% ylabel('Intensity (a.u.)','FontSize',30)



figure(14),hold on, box on
set(gcf,'Color',[1 1 1])
set(gca,'FontSize',30,'Xlim',[min(xplot)
max(xplot)],'Xdir','normal','Ylim',[-0.05 1])
% set(gca,'FontSize',30,'Xlim',[min(Time) max(Time)],'Ylim',[-0.05 1])
plot(xplot,band_sum_norm1,'r','linewidth',2)
plot(xplot,band_sum_norm2,'k','linewidth',2)
% plot(Time,band_sum_norm,'k','linewidth',2)
% xlabel('Annealing Temperature (^oC)','FontSize',30)
xlabel('Time (hours)','FontSize',30)
ylabel('Lane Normalized Intensity','FontSize',30)

%%
fileID = fopen("gel_data.txt",'w+');
for i=1:N
%
fprintf(fileID,'%4.2f\t%4.2f\t%4.3f\n',Time(i),band_sum(i),band_sum_norm(i));
fprintf(fileID,'%4.2f\t%4.2f\t%4.3f\t%4.2f\t%4.3f\n',xplot(i),band_sum1(i),ba
nd_sum_norm1(i),band_sum2(i),band_sum_norm2(i));
end
fclose(fileID);
```